Reaction $^{23}Na(\alpha,p)^{26}Mg$ from $E_\alpha = 2.3-3.7$ MeV and the corresponding thermonuclear reaction rate*

Daniel P. Whitmire and Cary N. Davids†
Center for Nuclear Studies, University of Texas, Austin, Texas 78712
(Received 29 October 1973)

Integrated excitation functions for the reactions $^{23}Na(\alpha,p_0)^{26}Mg$ and $^{23}Na(\alpha,p_1)^{26}Mg^*$ were measured over the energy range $E_\alpha = 2.3-3.7$ MeV. Absolute resonance strengths were determined for 30 new p_1 resonances and 9 new p_0 resonances. The corresponding stellar reaction rate $N_A\langle\sigma V\rangle$ is recalculated and found to be enhanced by a factor of 3 at $T_9 = 2$ and by a factor of 4 at $T_9 = 3$. A multiparameter analytic fit to the new $N_A\langle\sigma V\rangle$ as a function of temperature over the range $T_9 = 0.3-5.0$ is given. The enhanced rate was incorporated in a nucleosynthesis code and the resulting change in ^{23}Na and ^{26}Mg abundances at selected temperatures is discussed.

[NUCLEAR REACTIONS $^{23}Na(\alpha,p)$, $E = 2.3-3.7$ MeV; measured excitation function and deduced resonant strengths for p_0 and p_1 proton groups; NaCl target. Calculated new thermonuclear reaction rate.]

INTRODUCTION

During the helium-burning phase of stellar evolution the $3\alpha \rightarrow {}^{12}C$ reaction converts ^4He to ^{12}C. A significant amount of the ^{12}C goes to ^{16}O via $^{12}C(\alpha,\gamma)^{16}O$ before the ^4He is completely burned; hence, at the end of ^4He burning a carbon-oxygen core remains as fuel for the next phase of the star's evolution. The relative amounts of carbon and oxygen remaining at the end of core helium burning depend critically on the $^{12}C(\alpha,\gamma)^{16}O$ rate which is currently uncertain; however, it is usually thought that roughly equal amounts of carbon and oxygen are produced. For stars of mass $>1M_\odot$ the next phase of stellar evolution is carbon burning and this burning stage may occur either hydrostatically or explosively. The possible reaction products of carbon burning are:

$$^{12}C + {}^{12}C \rightarrow {}^{23}Na + p + 2.238\ \text{MeV},$$

$$^{12}C + {}^{12}C \rightarrow {}^{20}Ne + \alpha + 4.616\ \text{MeV},$$

$$^{12}C + {}^{12}C \rightarrow {}^{23}Mg + n - 2.605\ \text{MeV},$$

$$^{12}C + {}^{12}C \rightarrow {}^{24}Mg + \gamma + 13.930\ \text{MeV}.$$

The $^{23}Mg + n$ channel is inhibited by a negative Q value and the electromagnetic decay probability is always small relative to open particle channels. Hence, essentially all $^{12}C + {}^{12}C$ reactions proceed via the $^{23}Na + p$ and $^{20}Ne + \alpha$ channel. Once freed and thermalized the protons and α particles will interact with the other nuclei present such as the ^{23}Na and ^{20}Ne.

The present work was motivated by the lack of sufficient experimental data for the $^{23}Na(\alpha,p)^{26}Mg$ reaction. The stellar reaction rate has previously been calculated[1] on the basis of resonant strengths quoted by Kuperus[2] over the energy range $E_\alpha = 1.8-3.3$ MeV. However, this author measured only the yield of ground-state protons and there was reason to expect the proton yield leaving ^{26}Mg in its first excited state might be comparable to or much greater than the ground-state yield. A relative γ-ray yield from $^{23}Na(\alpha,p_1)^{26}Mg^*$ had previously been measured over the energy range $E_\alpha = 1.8-3.6$ MeV by Temmer and Heyenburg.[3] However, no cross section or resonant strengths were measured. The target employed was >40 keV thick and therefore these authors did not resolve most of the resonances reported in this work.

EXPERIMENTAL METHOD

A $^4He^+$ beam from the University of Texas 4-MV KN Van de Graaff accelerator was used to bombard a thin ($\simeq 25$-$\mu g/cm^2$) NaCl target evaporated on a thick copper slab. The copper slab was employed to help eliminate localized heating of the target. Since the melting temperature of NaCl is only 801°C, target deterioration was a constant problem at beam currents in excess of ~400 nA. Beam current during the experiment was maintained at ~400 nA and periodic checks were made to ensure that the target was not evaporating. The checks were made by comparing resonance peak yields, from the same resonance and target spot, after 10 to 20 h of bombardment. Experimentation with NaCl targets evaporated onto thin carbon foils, in the hope that the much smaller energy loss of the $^4He^+$ beam would offset the lower thermal con-

ductivity and strength of the carbon foils, proved unsuccessful. The carbon foils rapidly deteriorated when placed in the beam. The target normal was oriented at $-50°$ with respect to the beam.

Six 2200-μm lithium-drifted silicon solid-state detectors were cooled to liquid-nitrogen temperatures and positioned in a scattering chamber at laboratory angles of 45, 65, 85, 105, 125, and 145° with respect to the incident beam. The detectors were placed behind 7.6-cm-long barrels collimated at both ends to define the solid angle. Due to the thick copper-slab backing, only reflection geometry was possible. The data below 2.5 MeV were taken at five angles, the 125° detector being defective. Aluminum foils (0.01 cm thick) were placed over each collimator to suppress α particles and to ensure that only protons would be observed. The geometry was such that the beam spot was always clearly visible when viewed through the back collimator of each barrel. A 60-V positive bias was placed on the target to suppress electrons. It was found that the suppression was insensitive to the exact voltage applied in this range; this indicates that all knock-off electrons were suppressed. A biased collimator was placed in the beam line directly in front of the scattering chamber; it was found that the target current was completely independent of this bias voltage, implying that no electrons were hitting the target from upstream. An uncertainty of 5% is estimated in the absolute charge integration. The 5% is due entirely to inherent uncertainties in the integrator itself.

The signal from each detector went to a charge-sensitive Canberra model 806 preamplifier and on to a Tennelec 202 linear amplifier where the appropriate gain was set. From the linear amplifier the signal went to a Tennelec analog-to-digital converter (ADC) and then to a PDP-15 digital computer where the data were accumulated in 1024-channel spectra.

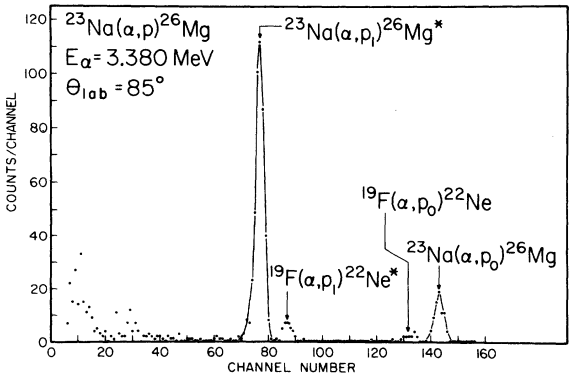

FIG. 1. A typical charged-particle spectrum.

Figure 1 shows a spectrum from a typical 400-μC run. The ^{19}F contaminant continuously built up on the beam spot, eventually necessitating a slight rotation of the target to a clean spot. When the beam spot was moved, appropriate checks were made to ensure that the new spot had the same ^{23}Na thickness as the old spot. The buildup was also found to be proportional to beam intensity (or heating) and vacuum pressure. Chamber vacuum pressure was maintained between 5×10^{-6} and 2×10^{-5} Torr measured at a diffusion pump directly beneath the scattering chamber. Protons from the $^{19}F(\alpha,p)^{22}Ne$ reaction had to be continuously monitored to ensure that they did not interfere with the ^{23}Na protons. The over-all resolution was ~100 keV and this was sufficient to resolve the ^{23}Na protons from the ^{19}F groups. All peaks were identified from the reaction kinematics after calculating the proton energy loss in the aluminum foils.

The accelerator analyzing magnet was calibrated from the $^7Li(p,n)^7Be$ threshold at 1.88 MeV. The magnetic field was measured using an NMR system. An uncertainty of ±10 keV in bombarding energy is estimated.

Angular distributions were normally taken in 4-keV intervals and fitted with a sum of four Legendre polynomials. The integrated yield is then proportional to A_0, where A_0 is the coefficient of $P_0(\cos\theta)$. The standard deviation in A_0 was typically less than 7% at resonant peaks. A relative integrated excitation function is shown for ground-state protons in Fig. 2 and first-excited-state protons in Fig. 3. Since these plots are of relative integrated yields the only uncertainty shown is due

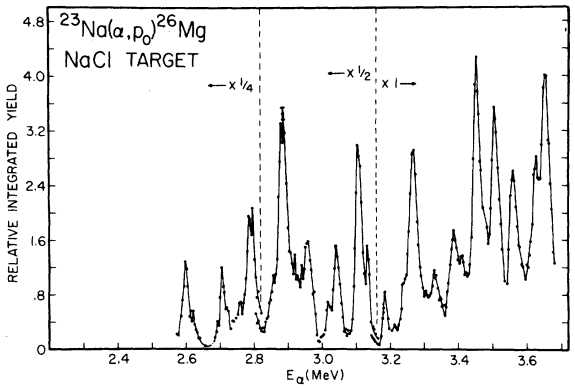

FIG. 2. The relative integrated yield of ground-state protons. Each point represents an integrated angular distribution. The NaCl target thickness is, in general, greater than the natural width of the resonances; therefore, the excitation function is not strictly proportional to the cross section. The most effective astrophysical energy E_0 is given as a function of temperatures in Table III.

to counting statistics. A total cross section was not obtained since most resonances have an observed width that reflects the target thickness. Resonant strengths were obtained for all 30 p_1 resonances and 9 new p_0 resonances, 8 of which were at energies >3.27 MeV and therefore not observed by Kuperus.[2] These strengths are tabulated in Tables I and II. The p_0 resonances at bombarding energies <3.27 MeV offered a means of comparing the present measurements with those of Kuperus.[2] Absolute strengths were determined by normalizing integrated resonance yields to a resonance with a known strength obtained from a thick-target yield. This procedure is described below.

The aluminum foils required to reduce the energy of α particles elastically scattered from the thick copper backing also act to degrade the proton energy. Since the stopping power varies inversely with energy it was not in general possible to resolve protons from higher excited states in ^{26}Mg. The proton yield leaving ^{26}Mg in its second excited state was observed at high energies ($E_\alpha \gtrsim 3.3$ MeV) and forward angles; the observed yield was comparable to the p_1 yield at these energies and angles. All other things being equal the lower penetrability of the p_2 group indicates that near the energies of astrophysical interest its contribution to the total yield should be less than the p_1 group (the first and second excited states in ^{26}Mg are 2^+).

TABLE I. Laboratory resonance strengths for new p_1 resonances.

E_α (lab) [a] (MeV)	$\omega\gamma$ (eV)	E_α (lab) (MeV)	$\omega\gamma$ (eV)
2.360	56^{+23}_{-10}	3.108	52^{+22}_{-9}
2.480	325^{+136}_{-58}	3.148	1017^{+417}_{-173}
2.539	676^{+277}_{-115}	3.200	521^{+214}_{-88}
2.619	201^{+84}_{-36}	3.262	1168^{+479}_{-198}
2.764	441^{+181}_{-75}	3.292	58^{+24}_{-10}
2.805	157^{+66}_{-28}	3.316	180^{+74}_{-31}
2.869	812^{+333}_{-138}	3.338	935^{+383}_{-159}
2.890	181^{+74}_{-31}	3.380	2319^{+951}_{-394}
2.940	515^{+211}_{-87}	3.420	1421^{+583}_{-242}
2.976	285^{+117}_{-48}	3.456	1246^{+511}_{-212}
2.992	85^{+35}_{-15}	3.488	1608^{+659}_{-273}
3.012	1235^{+506}_{-210}	3.556	1837^{+753}_{-312}
3.040	288^{+118}_{-49}	3.600	922^{+378}_{-157}
3.076	1037^{+425}_{-176}	3.628	1474^{+604}_{-251}
3.100	113^{+46}_{-19}	3.668	5047^{+2069}_{-858}

[a] All bombarding energies have an uncertainty of ±10 keV.

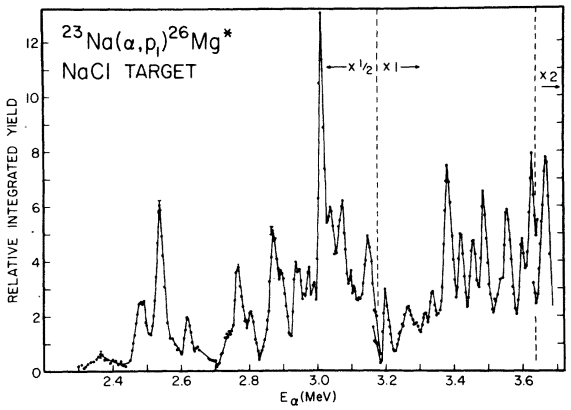

FIG. 3. The relative integrated yield of first-excited-state protons. Each point represents an integrated angular distribution. The NaCl target thickness is, in general, greater than the natural width of the resonances; therefore, the excitation function is not strictly proportional to the cross section. The most effective astrophysical energy E_0 is given as a function of temperature in Table III.

ANALYSIS

The ratio of the total integrated yields, Y, from two resonances is[4,5]

$$\frac{Y_1}{Y_2} = \frac{E_2}{E_1}\frac{(\omega\gamma)_1}{(\omega\gamma)_2}, \tag{1}$$

where E_1 and E_2 are the laboratory bombarding energies of the two resonances and $\omega\gamma$ is the resonance strength defined as[4]

$$\omega\gamma = (2J+1)\frac{\Gamma_1\Gamma_2}{\Gamma}. \tag{2}$$

TABLE II. Laboratory resonance strengths for new p_0 resonances.

E_α (lab) [a] (MeV)	$\omega\gamma$ (eV)
2.958	175^{+73}_{-31}
3.328	456^{+191}_{-82}
3.388	765^{+314}_{-130}
3.410	171^{+70}_{-29}
3.451	1262^{+517}_{-214}
3.505	1138^{+466}_{-193}
3.560	1008^{+413}_{-171}
3.622	811^{+332}_{-138}
3.652	1315^{+539}_{-224}

[a] All bombarding energies have an uncertainty of ±10 keV.

Here J is the resonance spin, Γ_1 is the partial width for the decay of the resonant state by re-emission of the bombarding particle, Γ_2 is the partial width for emission of the reaction particle, and Γ is the total width, $\Gamma = \Gamma_1 + \Gamma_2 + \cdots$, which is the sum over all partial widths. In the present case

$$\omega\gamma = (2J+1)\frac{\Gamma_\alpha \Gamma_p}{\Gamma} \simeq (2J+1)\Gamma_\alpha , \tag{3}$$

since $\Gamma = \Gamma_\alpha + \Gamma_p \simeq \Gamma_p$. From (1) it is evident that if a resonance strength and integrated yield are known for one resonance then a normalization factor can be obtained, and strengths for all other resonances determined by taking the ratio of their areas under the excitation curve to the area of the resonance with the known strength.

A thick-target yield over the p_0 resonance at 3.051 MeV was used to obtain an absolute strength. For a thick target $\omega\gamma$ is given in laboratory coordinates by[4,5]

$$\omega\gamma = (2J_{23}+1)(2J_\alpha+1)\frac{M_\alpha}{\pi^2\hbar^2}\epsilon(E_\alpha)\frac{e}{Q}E_\alpha Y(\infty), \tag{4}$$

where $Y(\infty)$ is the step in the thick-target integrated yield curve, J_{23} is the spin of ^{23}Na $(=\frac{3}{2})$, J_α is the spin of ^{4}He $(=0)$, M_α is the mass of ^{4}He, $\epsilon(E_\alpha)$ is the stopping cross section of NaCl in units of energy $\times$ length^2/atom, e is the electronic charge, and Q is the total charge collected. To a good approximation the ^{4}He equilibrium charge state in the target is +2,[6] (for $E_\alpha > 2$ MeV over 96% of the ^{4}He beam is in a +2 charge state) and to an accuracy of <1% the additivity property for compounds holds.[7] The tabulated stopping cross sections are estimated to be accurate within 1%, hence[8]

$$\epsilon_{\mathrm{NaCl}} = \epsilon_{\mathrm{Na}} + \frac{n_{Cl}}{n_{\mathrm{Na}}}\epsilon_{Cl} = \epsilon_{\mathrm{Na}} + \epsilon_{Cl}$$
$$= 74.2\ \mathrm{MeV\,cm^2/atom}, \tag{5}$$

where n is the number of atoms per cm^3. Making the appropriate substitutions into (4) gives

$$\omega\gamma = 150^{+61}_{-25}\ \mathrm{eV} \tag{6}$$

for the resonance at 3.051; all other absolute strengths were determined by normalizing to this resonance. This is in good agreement with the value of 170 eV quoted by Kuperus.[2] An uncertainty of ±25 eV in this number includes the uncertainty in charge collection, solid angle, stopping cross section, and statistics. It is known by the slope of the leading edge that $(\Gamma^2 + \Gamma_B^2)^{1/2} \leq 6.8$ keV for the 3.051 resonance; hence the observed width of ~22 keV insures that the thick-target approximation is a good one. Kuperus gives $\Gamma \leq 5$ keV for this resonance. An absolute minimum for ξ/Γ is $22/6.8 = 3.24$ and this corresponds to a (maximum yield)/(thick-target yield) of 0.809.[9] The fact that the target was only known with certainty to be $\geq 0.809\,Y(\infty)$ leads to a systematic uncertainty on upper error limit, and this is the origin of the asymmetric uncertainties quoted in Tables I and II.

THERMONUCLEAR REACTION RATE

The most effective astrophysical energy E_0 for a particular reaction represents a compromise between the Maxwell-Boltzman distribution $[\propto \sqrt{E}\, e^{-E/kT}]$ and the Gamow-Teller penetration factor $[\propto (1/E)e^{-bE^{-1/2}}]$ and is given by[10]:

$$E_0 = 1.22(Z_1^2 Z_2^2 A T_6^2)^{1/3}\mathrm{keV}, \tag{7}$$

where the Z's are the atomic numbers of target and projectile, A is the reduced atomic mass, and T_6 is the temperature in millions of degrees Kelvin. For ^{23}Na$(\alpha, p)^{26}$Mg, E_0 in laboratory coordinates is given for selected temperatures in Table III. It is evident that for explosive temperatures $>T_9 = 2$, it is possible to directly measure the appropriate experimental quantities in the laboratory without resorting to the extrapolation usually necessary at lower hydrostatic burning temperatures.

The center-of-momentum reaction rate per pair of particles is $\langle\sigma v\rangle$, where σ is the reaction cross section and v is the relative velocity. For a Maxwell-Boltzmann distribution it is given by

$$\langle\sigma v\rangle = \frac{(8/\pi)^{1/2}}{M^{1/2}(kT)^{3/2}}\int_0^\infty \sigma(E) E\, e^{-E/kT}\, dE, \tag{8}$$

where $\sigma(E)$ is the cross section as a function of energy, T is the temperature, and M the reduced mass. The effective spread in energy ΔE_0 is[10]

$$\Delta E_0 = 0.75(Z_1^2 Z_2^2 A T_6^5)^{1/6}\ \mathrm{keV}. \tag{9}$$

If the resonance is sharp, i.e., narrow relative to ΔE_0, $\langle\sigma v\rangle$ in (8) can be evaluated by substituting the Breit-Wigner dispersion relation

$$\sigma(E) = \frac{\pi\hbar^2}{2ME}\frac{\omega_r \Gamma_p \Gamma_\alpha}{(E-E_r)^2 + \Gamma^2/4} \tag{10}$$

into (8) and integrating. This gives, in center-of-momentum coordinates,[10]

$$\langle\sigma v\rangle = \left(\frac{2\pi\hbar^2}{MkT}\right)^{3/2}\frac{(\omega\gamma)_r}{\hbar}\, e^{-E_r/kT}. \tag{11}$$

TABLE III. The most effective energy E_0 as a function of temperature for the reaction ^{23}Na$(\alpha,p)^{26}$Mg. To convert to c.m. coordinates multiply by 23/27.

T_9	1.0	2.0	3.0	4.0	5.0
E_0 (MeV)	1.64	2.70	3.52	4.23	4.93

In the case of several isolated resonances

$$\langle \sigma v \rangle = \left(\frac{2\pi\hbar^2}{MkT}\right)^{3/2} \frac{1}{\hbar} \sum_r (\omega\gamma)_r e^{-E_r/kT}, \quad (12)$$

where $(\omega\gamma)_r = (2J+1)\Gamma_p\Gamma_\alpha/\Gamma$ as before, and the sum is over all resonances.

Equation (12) was used to calculate the quantity $N_A\langle \sigma v \rangle$, where N_A is Avogadro's number, at 16 temperatures between $T_9 = 0.3-5.0$. The calculation included all new resonances plus the previously used p_0 strengths from the data of Kuperus.[2] A small nonresonant and low-energy contribution, not shown in Tables I and II, was also used in the calculation of $N_A\langle \sigma v \rangle$. The nonresonant contribution comes from areas under the excitation curve that were not included as part of a resonance. The low-energy contribution represents a rough minimum estimate of the yield below 2.3 MeV from the excitation function given by Temmer and Heydenburg.[3] $N_A\langle \sigma v \rangle$ was then fitted to the multiparameter analytic function

$$N_A\langle \sigma v \rangle = AT_9^{-2/3} \exp(B/T_9^{1/3} + CT_9^2) + D\exp(E/T_9). \quad (13)$$

The constants were found to be: $A = 1.937\times10^{20}$, $B = -51.69$, $C = -1.663$, $D = 3.036\times10^6$, and $E = -22.72$; with an average uncertainty of 6% in the fit. $N_A\langle \sigma v \rangle$ is plotted as a function of temperature in Fig. 4. In Fig. 5 is plotted the ratio of the new $N_A\langle \sigma v \rangle$, given by (12) and the above constants, to the old value using just the p_0 strengths quoted by Kuperus.[2] It is seen, for example, that at the explosive temperature of $T_9 = 2$ the rate is enhanced by a factor of 3 and at $T_9 = 3$ by a factor of 4.

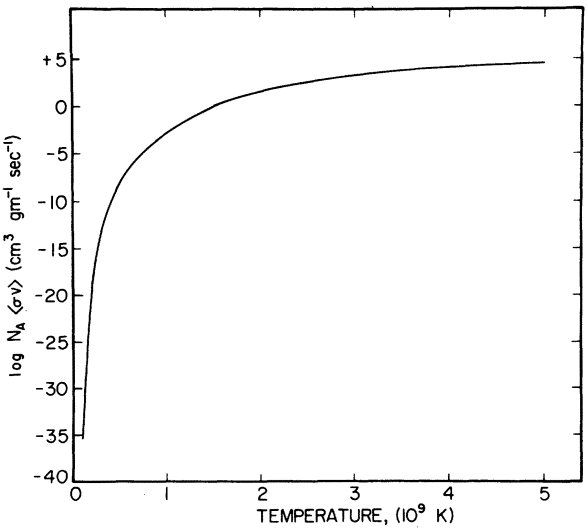

FIG. 4. The new thermonuclear reaction rate as a function of temperature.

DISCUSSION

The stellar reaction rate $N_A\langle \sigma v \rangle$ is significantly enhanced at temperatures appropriate to explosive carbon burning. The actual effect on isotopic abundances is, of course, model-dependent. In the case of explosive nucleosynthesis the parameters that influence final abundances are the peak temperature, peak density, expansion rate, and neutron excess. It is assumed that the expansion is nearly adiabatic, i.e.,

$$\rho T^{-3} \simeq \text{constant}, \quad (14)$$

and that ρ, and implicitly T, is given as a function of time by

$$\frac{1}{\rho}\left|\frac{d\rho}{dt}\right| \simeq (24\pi G\rho)^{1/2}, \quad (15)$$

where $(24\pi G\rho)^{1/2}$ is the gravitational free-fall rate. The neutron excess η is defined as

$$\eta \equiv \frac{n_n - n_p}{n_n + n_p} \quad (16)$$

and normally taken as 0.002, which corresponds to a solar composition. Typical peak temperatures for explosive nucleosynthesis calculations range from $\simeq T_9 = 2.0-2.6$, and peak densities are usually taken as $\rho = 10^4-10^5$ g/cm^3.

The new ^{23}Na$(\alpha, p)^{26}$Mg rate was included in an explosive carbon-burning nucleosynthesis code, similar to the one described by Arnett and Truran,[11] and calculations were carried out for temperatures of $T_9 = 2.0$, 2.2, 2.4, 2.6 and a density of $\rho = 10^5$ g/cm^3. Table IV gives the relative change in abundances of ^{23}Na and ^{26}Mg obtained from this calculation. It is seen that ^{26}Mg is increased by almost a factor of 2 at $T_9 = 2.4$, but is virtually unaffected at $T_9 = 2.0$. ^{23}Na is decreased by a factor of 1.3 at $T_9 = 2.0$ and is essentially unaffected at higher tem-

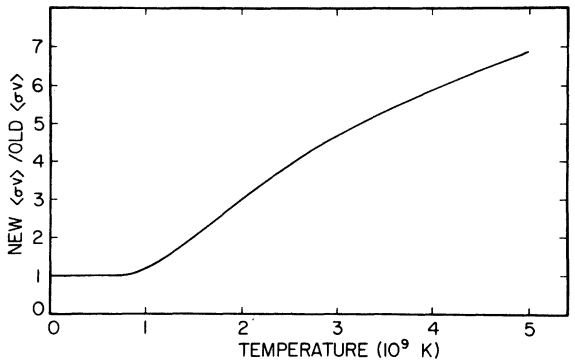

FIG. 5. The ratio of the new enhanced rate determined by the present work to the old rate as a function of temperature.

TABLE IV. The effect of the new reaction rate on calculated abundances ($X, Z \geq 6$) at selected temperatures for $\rho = 10^5$ g/cm^3. Abundances were calculated with an explosive nucleosynthesis code similar to the one discussed in Ref. 11.

T_9	2.0	2.2	2.4	2.6
^{26}Mg (new)	1.05×10^{-2}	1.30×10^{-3}	2.67×10^{-4}	9.9×10^{-5}
^{26}Mg (old)	1.02×10^{-2}	7.98×10^{-4}	1.47×10^{-4}	5.75×10^{-5}
^{23}Na (new)	1.71×10^{-3}	9.39×10^{-4}	2.40×10^{-4}	6.30×10^{-5}
^{23}Na (old)	2.15×10^{-3}	1.02×10^{-3}	2.54×10^{-4}	6.75×10^{-5}

peratures. Other abundances are also affected but to a lesser extent. The most recent (1973) "observed" abundances by Cameron[12] give $X_{23}(Z \geq 6) = 1.83\times10^{-3}$ and $X_{26}(Z \geq 6) = 4.076\times10^{-3}$, where $X_A(Z > 6)$ is the mass fraction of nucleus A relative to the sum of nuclear masses with $Z > 6$. It is evident from Table IV that for temperatures listed $> T_9 = 2.0$ the enhanced ^{26}Mg abundance gives a better agreement between the calculated and observed values. The decrease in the ^{23}Na abundance at $T_9 = 2.0$ is also in the proper direction for agreement between this calculation and Cameron's data. Higher temperatures have a negligible effect on ^{23}Na abundances.

It should be stressed that, for a given nuclear reaction rate, final calculated abundances are quite model-dependent. A different assumed η, expansion rate, peak temperature or density, a breakdown in the assumption of an adiabatic expansion, or subsequent new experimental measurements of relevant nuclear reaction rates may strongly affect the actual products of nucleosynthesis resulting from the new enhanced $^{23}Na(\alpha, p)^{26}Mg$ rate.

We acknowledge Dr. Richard G. Couch for several valuable suggestions. Thanks are due J. Loveless, R. Pardo, L. Parks, and A. Schmiedekamp for help in taking and reducing the data.

*Work supported in part by the National Science Foundation and the Robert A. Welch Foundation.

†Alfred P. Sloan Foundation Fellow.

[1]W. A. Fowler, G. R. Caughlan, and B. A. Zimmerman, to be published.

[2]J. Kuperus, Physica 30, 2252 (1964).

[3]G. M. Temmer and N. P. Heydenburg, Phys. Rev. 96, 426 (1954).

[4]P. B. Lyons, J. W. Toevs, and D. G. Sargood, Nucl. Phys. A130, 1 (1969).

[5]H. E. Give, in *Nuclear Reactions*, edited by P. M. Endt and M. Demeur (North-Holland, Amsterdam, 1959), Vol. 1, p. 302.

[6]J. B. Marion and F. C. Young, *Nuclear Reaction Analysis* (American Elsevier, New York, 1968), p. 37.

[7]J. F. Janni, Air Force Weapons Laboratory, Kirtland Air Force Base, New Mexico, Technical Report No. AFWL-TR-65-150, 1966 (unpublished).

[8]H. E. Gove, Ref. 7, p. 304.

[9]W. A. Fowler, C. C. Lauritsen, and T. Lauritsen, Rev. Mod. Phys. 20, 236 (1948).

[10]D. D. Clayton, *Principles of Stellar Evolution and Nucleosynthesis* (McGraw-Hill, New York, 1968), Chap. 4.

[11]W. D. Arnett and J. W. Truran, Astrophys. J. 157, 339 (1969).

[12]A. G. W. Cameron, in *Explosive Nucleosynthesis*, edited by D. N. Schramm and W. D. Arnett (University of Texas Press, Austin, 1973), p. 3.